Effect of primordial non-Gaussianity on halo bias and mass function

Desjacques, V ; Seljak, U ; Iliev, I T

Abstract: We discuss the effect of quadratic and cubic local non-Gaussianity on the mass function and bias of dark matter halos extracted from cosmological N-body simulations. This type of non-Gaussianity induces a k-dependent bias in the large-scale clustering of rare objects. While we find that at low wavenumbers k<0.03 hMpc-1 the theory and the simulations agree well with each other for biased halos with b(M)>1.5, including a scale independent correction to the non-Gaussian bias improves the agreement on small scales where the k-dependent effect becomes rapidly negligible. Using available large-scale structure data, we obtain a limit on the size of the cubic nonlinear parameter of -3.5×105< gNL<8.2×105. Future observations shall improve this bound by 1-2 orders of magnitude.

DOI: https://doi.org/10.1063/1.3462723

Effect of primordial non-Gaussianity on halo bias and mass function

Vincent Desjacques, Uroš Seljak, and Ilian T. Iliev

Citation: AIP Conference Proceedings **1241**, 826 (2010); doi: 10.1063/1.3462723
View online: http://dx.doi.org/10.1063/1.3462723
View Table of Contents: http://scitation.aip.org/content/aip/proceeding/aipcp/1241?ver=pdfcov
Published by the AIP Publishing

Effect of primordial non-Gaussianity on halo bias and mass function

Vincent Desjacques*, Uroš Seljak*,† and Ilian T. Iliev*,**

*Institute for Theoretical Physics, University of Zürich, Winterthurerstrasse 190, CH-8057 Zürich, Switzerland
†Physics and Astronomy Department, University of California, and Lawrence Berkeley National Laboratory, Berkeley, California 94720, USA
**Astronomy Centre, Department of Physics & Astronomy, University of Sussex, Brighton BN1 9QH, UK

Abstract.
We discuss the effect of quadratic and cubic local non-Gaussianity on the mass function and bias of dark matter halos extracted from cosmological N-body simulations. This type of non-Gaussianity induces a k-dependent bias in the large-scale clustering of rare objects. While we find that at low wavenumbers $k < 0.03\,h\mathrm{Mpc}^{-1}$ the theory and the simulations agree well with each other for biased halos with $b(M) > 1.5$, including a scale independent correction to the non-Gaussian bias improves the agreement on small scales where the k-dependent effect becomes rapidly negligible. Using available large-scale structure data, we obtain a limit on the size of the cubic nonlinear parameter of $-3.5\times10^5 < g_{\rm NL} < 8.2\times10^5$. Future observations shall improve this bound by 1-2 orders of magnitude.

Keywords: large-scale structures, dark matter, primordial non-Gaussianity
PACS: 98.80.-k, 98.80.Cq, 98.80.Es, 98.70.Vc

INTRODUCTION

A wide class of inflationary scenarios lead to non-Gaussianity of the local type, i.e. which depends on the local value of the primordial curvature perturbation (Here and henceforth, the usual Bardeen potential in matter-dominated era). In these models, deviation from Gaussianity can be conveniently parametrised up to the third order as

$$\Phi(\mathbf{x}) = \phi(\mathbf{x}) + f_{\rm NL}\phi(\mathbf{x})^2 + g_{\rm NL}\phi(\mathbf{x})^3\,, \tag{1}$$

where $\phi(\mathbf{x})$ is an isotropic Gaussian random field whose power spectrum is a power-law $P_\phi(k) \sim k^{n_s-4}$, whereas $f_{\rm NL}$ and $g_{\rm NL}$ are the quadratic and cubic nonlinear parameters. The nonlinear corrections are small since curvature perturbations are typically $\mathcal{O}(10^{-5})$.

The cosmic microwave background (CMB) and large scale structures (LSS) offer two different avenue to constrain the magnitude of the non-Gaussian contribution. The main advantage of the CMB resides in the fact that the observed spherical harmonics coefficient a_l^m are a linear superposition of the primordial curvature perturbations (weighted by the radiation transfer function). Therefore, any non-zero three-point and/or higher correlation function of $\Phi(\mathbf{x})$ is directly mirrored in the corresponding statistics of the primary temperature anisotropies. Thus far, analysis of the CMB three-point function indicates that the data is fully consistent with Gaussianity, with $-9 < f_{\rm NL} < +111$ at 95% C.L. [1]. No observational limits have been set on $g_{\rm NL}$ by measuring the CMB four-point function. Nevertheless, since the current bound on $f_{\rm NL}$ implies a relative contribution for the quadratic term of ~ 0.1 per cent, a third order coupling parameter $|g_{\rm NL}| \sim 10^6$ is expected to be consistent with the data.

Unlike the CMB, nonlinear gravitational evolution of LSS can significantly contaminate the signal due to primordial non-Gaussianity. However, causality implies that this contamination decays rapidly as one goes to large distances. Another important difference with the CMB is that LSS are traced by galaxies etc. which are biased relative to the matter distribution (since these preferentially form in overdense regions). As a consequence of this bias relation, high order statistics of the matter density field (such as the three-point function) can project onto low order statistics of biased tracers (such as the power spectrum). In particular, Ref. [2, 3, 4] showed that the three-point function for the local quadratic coupling $f_{\rm NL}\phi^2$ induces a scale dependent bias $\Delta b_\kappa(k, f_{\rm NL})$ in the large-scale power spectrum of biased tracers,

$$\Delta b_\kappa(k, f_{\rm NL}) = 3 f_{\rm NL}\,[b(M)-1]\,\delta_{\rm c}\frac{\Omega_{\rm m}H_0^2}{k^2 T(k) D(z)}\,, \tag{2}$$

CP1241, *Invisible Universe: Proceedings of the Conference,* edited by J.-M. Alimi and A. Füzfa

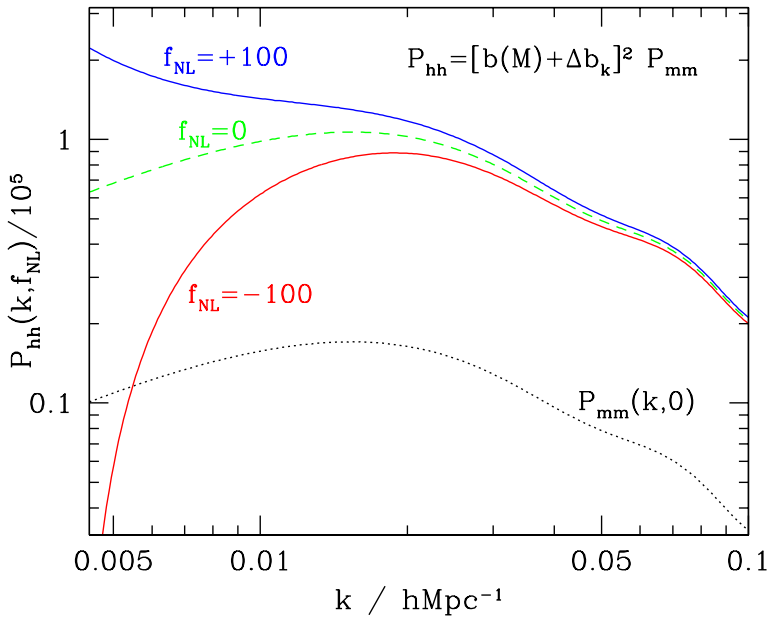

FIGURE 1. Scale dependent bias correction induced by primordial non-Gaussianity of the local, $f_{\rm NL}$-type in the power spectrum of biased tracers with linear bias $b = 2$. Results are shown at redshift $z = 0$ for $f_{\rm NL} = 0, \pm 100$ and $g_{\rm NL} = 0$. The dotted curve is the matter power spectrum.

where $b(M)$ is the linear bias parameter, H_0 is the Hubble parameter, $T(k)$ is the matter transfer function normalised to unity as $k \to 0$, $D(z)$ is the growth factor normalised to $(1+z)^{-1}$ in the matter era and $\delta_{\rm c} \sim 1.68$ is the present-day (linear) critical density threshold. Figure 1 illustrates the effect for a population of linear bias $b = 2$ at $z = 0$.

Ref. [4] applied this relation to constrain the value of $f_{\rm NL}$ using a compilation of large-scale structures data and found limits comparable to those from WMAP5, $-29 < f_{\rm NL} < +69$. The method looks promising: future galaxy redshift surveys shall achieve constraints of the order of unity [5, 6, 7, 8].

On the numerical side however, the exact amplitude of the non-Gaussian bias correction remains somewhat debatable. Furthermore, all numerical studies to date have only implemented the quadratic term $f_{\rm NL}\phi^2$. For these reasons, we have tested the theoretical prediction (2) against the outcome of large cosmological simulations. We have also extended the analysis to the cubic coupling to derive limits on the nonlinear parameter $g_{\rm NL}$.

N-BODY SIMULATIONS

We utilise a series of large N-body (collisionless) simulations of the ΛCDM cosmology seeded with Gaussian and non-Gaussian initial conditions. We adopt the standard (CMB) convention in which the Bardeen potential $\Phi(\mathbf{x})$ is primordial, and not extrapolated to present epoch. We run five sets of five 1024^3 simulations, each of which has $(f_{\rm NL}, g_{\rm NL}) = (0,0)$, $(\pm 100, 0)$ and $(0, \pm 10^6)$. We use the same Gaussian random seed field ϕ in each set of runs so as to minimise the sampling variance. The box size, 1600 h^{-1}Mpc, is large enough to contain many long wavelength modes for which the effect is strongest. At the same time, the particle mass is 3.0×10^{11} $\mathrm{M}_\odot/h$, enough to resolve halos of mass 10^{13} $\mathrm{M}_\odot/h$ hosting the surveyed galaxies and QSOs (quasars).

We interpolate the dark matter particles and halo centres onto a regular 512^3 mesh, whose Nyquist wavenumber is sufficiently large (≈ 1 hMpc^{-1}) to allow for an accurate measurement of the power in wavemodes of amplitude $k \lesssim 0.1$ hMpc^{-1}. The resulting dark matter and halo fluctuation fields are then Fourier transformed to yield the matter-matter, halo-matter and halo-halo power spectra $P_{\rm mm}(k)$, $P_{\rm mh}(k)$ and $P_{\rm hh}(k)$, respectively. These power spectra are measured for various halo masses and redshifts, covering a range of statistical properties corresponding to those of the available galaxy or QSO populations with different luminosities and bias. Note that the magnitude of the k-dependent

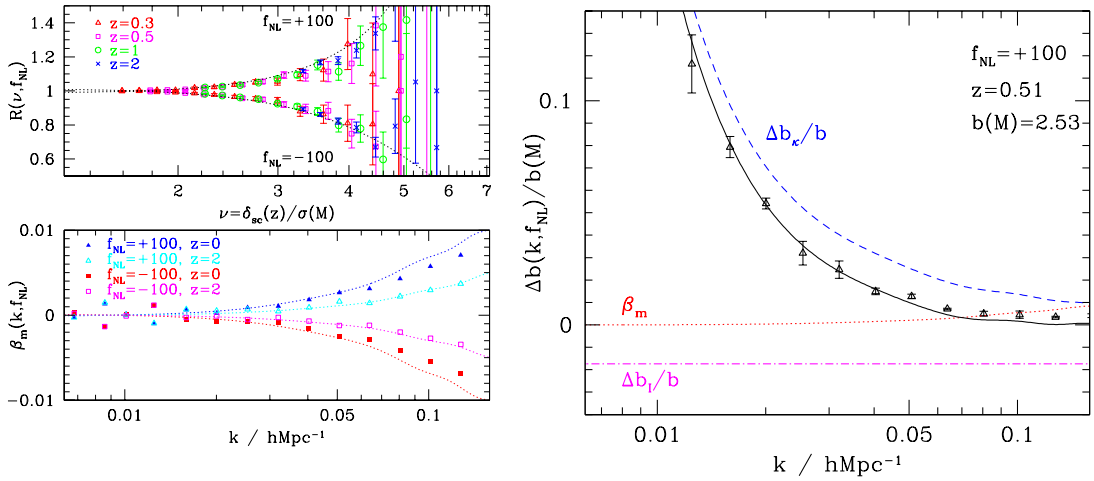

FIGURE 2. Fractional deviation from the fiducial Gaussian mass function (upper left) and Gaussian matter power spectrum (lower left). Different symbols refer to different models and redshifts as indicated. The dotted curves show theoretical predictions. These effects induce two additional corrections to the halo bias shown in the right panel. Our theoretical scaling Eq. (5) (solid curve) agrees very well with the data for $k \lesssim 0.05\ h\mathrm{Mpc}^{-1}$.

non-Gaussian bias (2) crucially depends upon the linear halo bias $b(M)$. We use the ratio $P_{\rm mh}(k)/P_{\rm mm}(k)$ as a proxy for $b(M)$ since it is less sensitive to shot-noise.

In order to quantify the effect of non-Gaussianity on the halo bias, we consider the ratios

$$\begin{aligned} \frac{P_{\rm mh}(k,f_{\rm NL},g_{\rm NL})}{P_{\rm mh}(k,0)} - 1 &= \frac{\Delta b(k,f_{\rm NL},g_{\rm NL})}{b(M)} \\ \frac{P_{\rm hh}(k,f_{\rm NL},g_{\rm NL})}{P_{\rm hh}(k,0)} - 1 &= \left(1+\frac{\Delta b(k,f_{\rm NL},g_{\rm NL})}{b(M)}\right)^2 - 1\,, \end{aligned} \tag{3}$$

where $\Delta b(k,f_{\rm NL},g_{\rm NL})$ is the non-Gaussian bias. Although $P_{\rm mh}$ is less affected by discreteness, it is important to measure the effect in the auto-power spectrum $P_{\rm hh}$ of dark matter halos since the latter gives the strongest constraint on the nonlinear parameters.

NON-GAUSSIAN BIAS SHIFT IN $f_{\rm NL}$ MODELS

Let us first consider the simulations with non-vanishing $f_{\rm NL}$ only. At the lowest order, there are two additional, albeit relatively smaller, corrections to the halo bias which arise from the dependence of both the halo number density $n(M,z)$ and the matter power spectrum $P_{\rm mm}$ on the nonlinear parameter $f_{\rm NL}$ [9].

Assuming the peak-background split holds, the change in the mean number density of halos induces a k-independent shift

$$\Delta b_{\rm I}(f_{\rm NL}) = -\frac{1}{\sigma}\frac{\partial}{\partial\nu}\ln\left[R(\nu,f_{\rm NL})\right] \tag{4}$$

where $\nu = \delta_{\rm c}(z)/\sigma(M)$ is the peak height at mass scale M and $R(\nu,f_{\rm NL})$ is the fractional correction to the Gaussian mass function. Notice that $\Delta b_{\rm I}(f_{\rm NL})$ has a sign opposite to that of $f_{\rm NL}$, because the bias decreases when the mass function goes up as can be seen in the upper left panel of Fig.2).

The quadratic coupling also affects the matter power spectrum as positive values of $f_{\rm NL}$ tend to increase the small-scale power. For $|f_{\rm NL}| = 100$, the magnitude of the fractional correction $\beta_{\rm m}(k,f_{\rm NL}) = P_{\rm mm}(k,f_{\rm NL})/P_{\rm mm}(k,0) - 1$ is at a per cent level in the weakly nonlinear regime $k \lesssim 0.1\ h\mathrm{Mpc}^{-1}$. The lower left panel of Fig.2 demonstrates that leading order perturbation theory [10] provides an excellent description of the effect over the wavenumbers of interest, $k \lesssim 0.1\ h\mathrm{Mpc}^{-1}$.

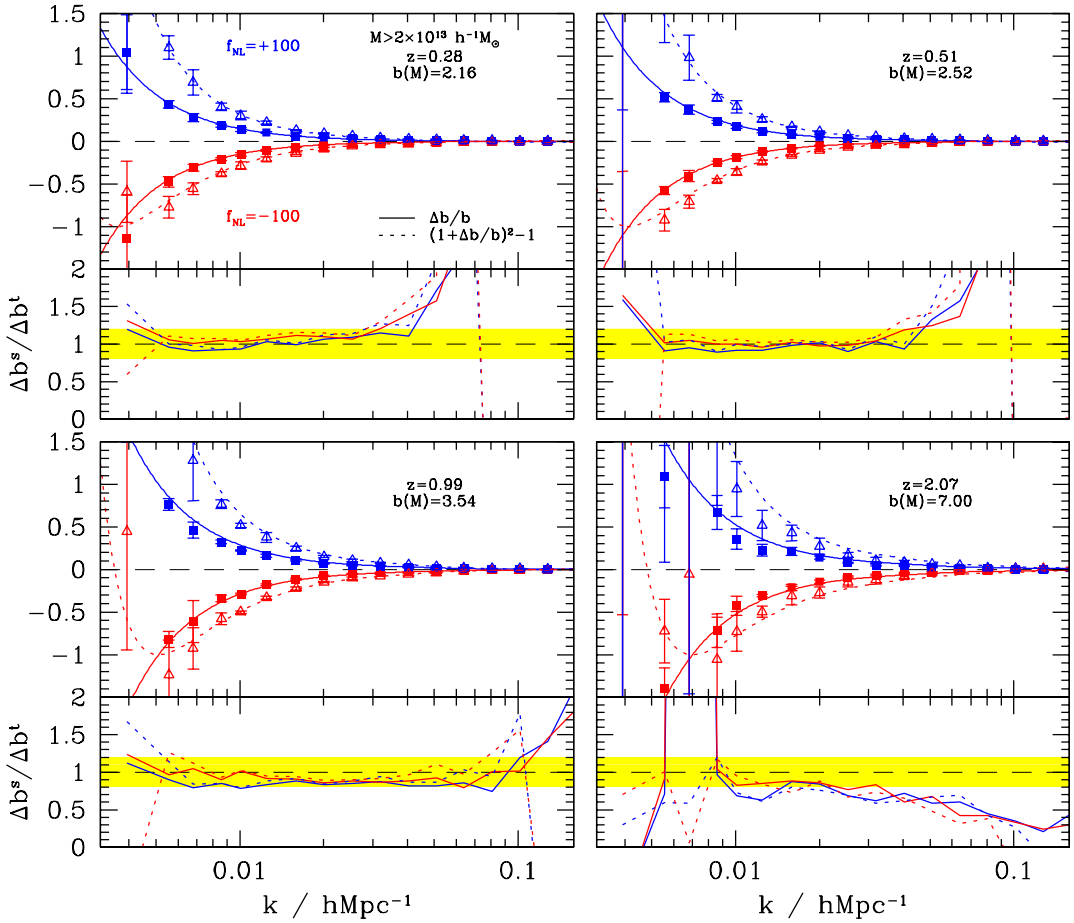

FIGURE 3. Non-Gaussian bias correction for halos of mass $M > 2 \times 10^{13}\ \mathrm{M}_\odot/h$. In each panel, the upper window shows the ratio $P_{\rm hh}(k, f_{\rm NL})/P_{\rm hh}(k,0) - 1$ (dotted curves, empty symbols) and $P_{\rm mh}(k, f_{\rm NL})/P_{\rm mh}(k,0) - 1$ (solid curves, filled symbols), while the lower window displays the departure from the theoretical prediction. The errors bars represent the scatter among 5 realisations.

Summarising, local non-Gaussianity of the $f_{\rm NL}$-type adds a correction $\Delta b(k, f_{\rm NL})$ to the bias $b(k)$ of dark matter halos that can be written as

$$\Delta b(k, f_{\rm NL}) = \Delta b_\kappa(k, f_{\rm NL}) + \Delta b_{\rm I}(f_{\rm NL}) + b(M)\beta_{\rm m}(k, f_{\rm NL}) \tag{5}$$

at the first order. The right panel of Fig. 2 illustrates the relative contribution of these terms for halos of mass $M > 2 \times 10^{13}\ \mathrm{M}_\odot/h$ identified at redshift $z = 0.5$. The data points are obtained from measurements of the cross-power spectrum in the N-body simulations. The solid curve shows the total non-Gaussian bias $\Delta b(k, f_{\rm NL})$. Considering only the scale dependent shift Δb_κ leads to an apparent suppression of the effect in simulations relative to the theory. Including the scale independent correction $\Delta b_{\rm I}$ considerably improves the agreement at wavenumbers $k \lesssim 0.05\ h\mathrm{Mpc}^{-1}$. Finally, adding the scale dependent term $b(M)\beta_{\rm m}$ further adjusts the match at small scale $k \gtrsim 0.05\ h\mathrm{Mpc}^{-1}$ by making the non-Gaussian bias shift less negative.

If halos and dark matter do not trace each other on large scales, i.e. if there is stochasticity, then analyses based on the auto- and cross-power spectrum may not agree with each other. While models with Gaussian initial conditions predict little stochasticity on large scales, this has not been shown for models with non-Gaussianity. Figure 3 shows that measurements of the non-Gaussian bias correction obtained with the halo-halo or the halo-matter power spectrum are

in a good agreement with each other, suggesting that non-Gaussianity does not induce stochasticity and the predicted scaling applies equally well for the auto- and cross-power spectrum.

For highly biased halos ($b(M) \gtrsim 1.5$), our results indicate that the simulated non-Gaussian bias converges towards the theoretical prediction on scales $k \lesssim 0.03\ h\mathrm{Mpc}^{-1}$. At larger wavenumbers, the effect depends strongly on scale independent bias. If we include this contribution using the analytic formula, Eq. (4), the suppression relative to theory is much smaller and, in some cases, goes in the opposite direction. Still, one could argue that scale independent bias cannot be identified from the data alone, so one should fit for it and include it in the overall bias, as was done in [4]. In this case, the agreement between theory and simulations is improved further. Finally, for the halo samples with $b(M) \lesssim 1.5$ there is some evidence that the actual bias exceeds the theory on all scales. Therefore, the proposed scaling does not appear to be universal, so care must be exercised when applying Eq. (5) to the actual LSS data.

EFFECT OF A NON-ZERO CUBIC COUPLING

If $\mathscr{O}(f_{\rm NL}) \sim \mathscr{O}(g_{\rm NL})$ then the cubic correction should always be negligibly small compared to the quadratic one. However, this condition is not satisfied by some multifield inflationary models such as the curvaton scenario for instance, in which a large $g_{\rm NL}$ and a small $f_{\rm NL}$ can be simultaneously produced [11, 12, 13, 14, 15, 16, 17].

Non-Gaussian mass functions and bias

The cubic order term $g_{\rm NL}\phi^3$ brings about an additional subtlety as it renormalizes the amplitude A_ϕ of the power spectrum of initial curvature perturbations to $A_\phi \rightarrow A_\phi + 6g_{\rm NL}\langle\phi^2\rangle$. In terms of the normalisation amplitude σ_8, this amounts to a change

$$\delta\sigma_8 \approx 0.015\left(\frac{g_{\rm NL}}{10^6}\right) . \tag{6}$$

This correction is fairly large for the values of $g_{\rm NL}$ adopted here and, therefore, must be taken into account in the comparison between the theory and the simulations. As we will see below, this is especially important when studying the high mass tail of the halo mass function which is exponentially sensitive to the amplitude of density fluctuations.

Mass function

The fractional deviation from Gaussianity can be modelled accurately using the Press-Schechter formalism [18]. In this approach, the halo mass function $n(M,z)$ is related to the probability $P(>\delta_{\rm c},M)$ that a region of mass M exceeds the critical linear density for collapse $\delta_{\rm c}(z)$ through the relation $n(M,z) = -2\,(\bar{\rho}/M)\,dP/dM$, where $\bar{\rho}$ is the average matter density. The non-Gaussian fractional correction to the multiplicity function then is $R(\nu,g_{\rm NL}) \equiv f(\nu,g_{\rm NL})/f(\nu,0) = (dP/dM)(>\delta_{\rm c},M,g_{\rm NL})/(dP/dM)(>\delta_{\rm c},M,0)$. Following the approach adopted in [19, 20], in which $P(\delta_M)$ is expressed as the inverse transform of a cumulant generating function, we derive the first order approximation [21]

$$R(\nu,g_{\rm NL}) = \exp\left[\frac{\nu^4}{4!}\sigma^2 S_4 + \nu^2\delta\sigma_8\right]\left\{1 - \frac{\nu^2}{4}\sigma^2 S_4 - \frac{\nu^2}{4!}\frac{d(\sigma^2 S_4)}{d\ln\nu}\right\} . \tag{7}$$

In Fig.4, the fractional correction is plotted for the halos extracted from the simulation outputs at $z = 0.3$, 0.5, 1 and 2. As we can see, Eq. (7) performs reasonably well regardless of the sign of $g_{\rm NL}$. The discrepancy somewhat worsens at higher redshift, especially in the case $g_{\rm NL} = 10^6$. It is possible the agreement may be improved by adding higher order powers of $\sigma^2 S_4$ and higher order cumulants. One should also keep in mind that all these extensions are based on Press-Schechter theory and, therefore, provide a bad fit to the Gaussian mass function of halos. In this respect, excursion set approaches may be more promising since they seem to reproduce both the Gaussian halo counts and the dependence on $f_{\rm NL}$ [22].

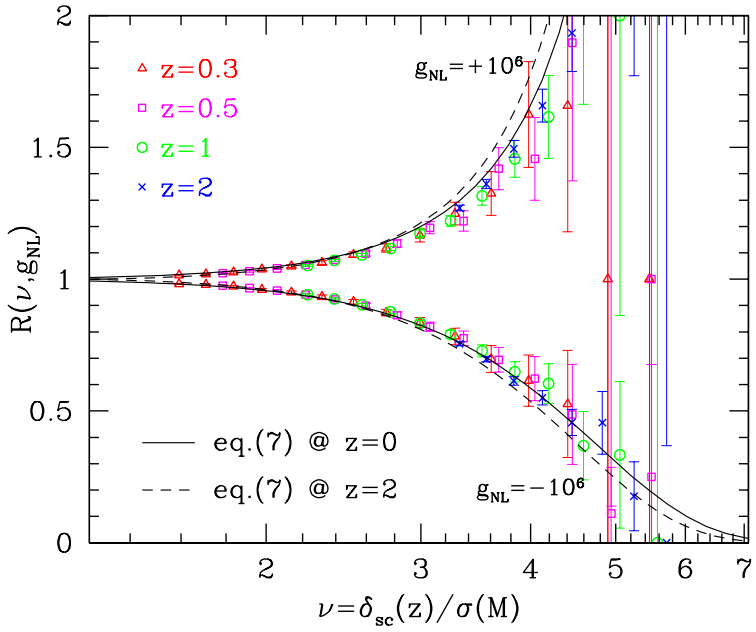

FIGURE 4. Fractional correction to the Gaussian multiplicity function of dark matter halos as a function of the peak height $\nu(M,z)$ for the models with $g_{\rm NL}=\pm10^6$. The solid and dashed curves show the theoretical prediction, Eq. (7), at redshift $z=0$ and 2, respectively.

Bias

The scale dependent bias correction to the power spectrum of dark matter halos induced by the cubic coupling term can also be derived from the statistics of Lagrangian regions above $\delta_{\rm c}(z)$. In the limit of long wavelength $k\ll1$, the scale dependent bias correction can be cast into the form [21]

$$\begin{aligned}\Delta b_\kappa(k,g_{\rm NL}) &= \frac{3}{4}g_{\rm NL}b_{\rm L}(z)\delta_c^2(0)\frac{D(0)}{D(z)^2}S_3^{(1)}(M)\frac{\Omega_{\rm m}H_0^2}{k^2T(k)} \\ &= \frac{1}{4}g_{\rm NL}\delta_c(z)S_3^{(1)}(M)\Delta b_\kappa(k,f_{\rm NL}=1)\,,\end{aligned} \tag{8}$$

where $\Delta b_\kappa(k,f_{\rm NL})$ is the scale independent bias induced by the quadratic coupling $f_{\rm NL}\phi^2$, Eq. (2), and $S_3^{(1)}(M)$ is the normalised skewness. We have also assumed the Eulerian bias prescription $b(M)=1+b_{\rm L}(M)$. The change in the mean number density of halos also creates a scale independent shift which we denote by $\Delta b_{\rm I}(g_{\rm NL})$. However, the scale dependent correction in the matter power spectrum, $\beta_{\rm m}(k,g_{\rm NL})$, is very small and can be safely neglected.

We find that a non-Gaussian bias of the form $\Delta b(k,g_{\rm NL})=\Delta b_\kappa(k,g_{\rm NL})+\Delta b_{\rm I}(g_{\rm NL})$ significantly overestimates the magnitude of the effect measured in the simulations. Assuming that the scaling $k^{-2}T(k)^{-1}$ still holds, we consider instead the phenomenological relation

$$\Delta b(k,g_{\rm NL})=\varepsilon_\kappa\,\Delta b_\kappa(k,g_{\rm NL})+[\Delta b_{\rm I}(g_{\rm NL})+\varepsilon_{\rm I}]\,, \tag{9}$$

and treat ε_κ and $\varepsilon_{\rm I}$ as free parameters that we fit to our measurements of the cross-power spectrum in the range $0.005\le k\le0.03\,h{\rm Mpc}^{-1}$ where the scale dependent effect is largest. Figure 5 shows the resulting best-fit contributions $\varepsilon_\kappa\Delta b_\kappa$ and $\Delta b_{\rm I}+\varepsilon_{\rm I}$ for the halo sample mentioned above. As can be seen, ε_κ and $\varepsilon_{\rm I}$ appear to depend mainly upon the linear halo bias $b(M)$ and the coupling parameter $g_{\rm NL}$, although dependencies on redshift or other halo observables are not excluded (The data is too noisy for a reliable estimate of these). More precisely, ε_κ is a monotonically increasing function of the bias and never reaches unity, even for the most biased samples for which the high peak approximation should be valid. Furthermore, ε_κ is noticeably larger for $g_{\rm NL}=-10^6$, suggesting thereby that second (and higher) order

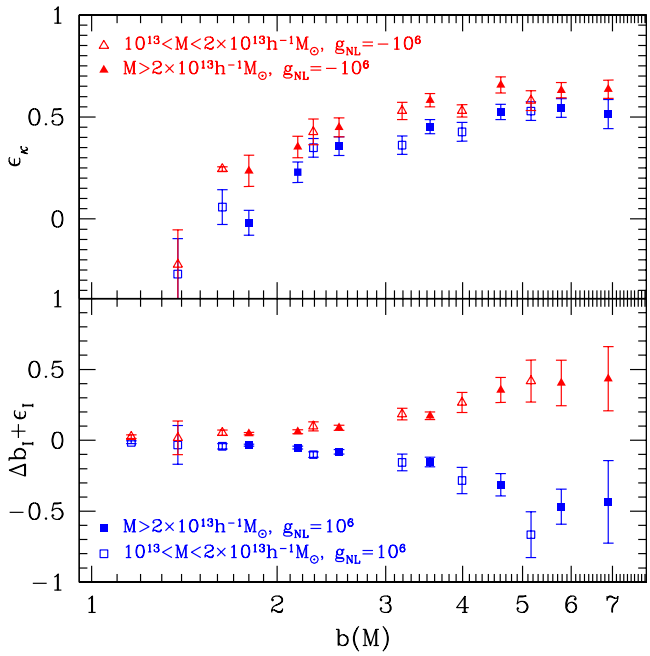

FIGURE 5. Best-fitting values of ε_κ (top) and $\Delta b_I + \varepsilon_I$ (bottom) as a function of halo bias for $g_{NL} = \pm 10^6$ and for two different mass cuts as indicated in the Figure.

contributions to the scale dependent bias may be important. For $b \lesssim 1.5$ where the high peak approximation breaks down, there is evidence that the effect reverses sign. The scale independent correction $\Delta b_I + \varepsilon_I$ has sign opposite to that of g_{NL}, in agreement with theoretical expectations from the peak-background split. However, whereas for $b \lesssim 3$ the magnitude of the correction is comparable to that predicted by the peak-background split, it is considerably larger for $b \gtrsim 3$, reaching up to 5-10 per cent of the linear halo bias.

Constraints on g_{NL} from current large-scale structure data

Ref. [4] took advantage of the scale dependence of the bias to constrain f_{NL} from a sample of highly biased LRGs (luminous red galaxies) and QSOs. It is straightforward to translate their 2-σ limit $-29 < f_{NL} < +69$ into a constraint on g_{NL} since the non-Gaussian scale dependent bias $\Delta b_\kappa(k, g_{NL})$ has the same functional form as $\Delta b_\kappa(k, f_{NL})$.

Constraints will arise mostly from the QSO sample at median redshift $z = 1.8$, which covers a large comoving volume and is highly biased, $b = 2.7$. In light of our results, we expect the parameter $\varepsilon_\kappa(b, g_{NL})$ to vary with g_{NL}. However, in order to simplify the analysis, we will assume that, at fixed b, $\varepsilon_\kappa(b, g_{NL})$ is given by the mean of $\varepsilon_\kappa(b, g_{NL} = \pm 10^6)$. For a sample with bias $b \sim 2.7$, this yields $\varepsilon_\kappa \simeq 0.4$. Furthermore, assuming $M \sim 10^{13}\ M_\odot/h$ for the typical mass of QSO-hosting halos gives $S_3^{(1)}(M) \simeq 2.3 \times 10^{-4}$. As a result, the multiplicative factor $(1/4)\,\delta_c(z)\varepsilon_\kappa S_3^{(1)}(M)$ is approximately $\simeq 8.4 \times 10^{-5}$. Our limits on g_{NL} thus are

$$-3.5 \times 10^5 < g_{NL} < +8.2 \times 10^5 \tag{10}$$

at 95% confidence level. For the limits obtained here, $|\Delta b_I + \varepsilon_I|$ should be much smaller than b and can thus be ignored. Note also that, whereas the non-Gaussian bias scales as $D(z)^{-1}$ in f_{NL} models, we have $\Delta b(k, g_{NL}) \propto D(z)^{-2}$ for g_{NL} non-Gaussianity (Eq. (9)), so one can achieve relatively larger gains on g_{NL} from measurements of high redshift tracers.

Predictions for future LSS surveys

We can estimate the detection limit for $g_{\rm NL}$ that could be reached with future galaxy surveys. Considering a (nearly spherical) survey of volume V and assuming the Fourier modes are still uncorrelated and Gaussian distributed, the total signal-to-noise squared reads

$$\left(\frac{S}{N}\right)^2 \approx \frac{V}{4\pi^2}\int_{k_{\rm min}}^{k_{\rm max}} dk\, k^2 \left[\left(1+\frac{\Delta b_\kappa}{b}\right)^2 - 1\right]^2 \tag{11}$$

in the limit where sampling variance dominates the errors. Here, $k_{\rm min}\sim \pi/V^{1/3}$ is the smallest wavemode accessible and $k_{\rm max}$ is not necessarily finite since the integral does converge as one takes $k_{\rm max}$ to infinity. Substituting the expression (8) for the scale dependent bias $\Delta b_\kappa(k, g_{\rm NL})$ and setting $T(k)\equiv 1$ over the wavenumber range across which the integral is performed, we arrive at

$$\left(\frac{S}{N}\right)^2 \approx 8.1\times 10^{-13} g_{\rm NL}^2 \varepsilon_\kappa^2 \left(1-\frac{1}{b}\right)^2 D(z)^{-4} \left(\frac{S_3^{(1)}}{10^{-4}}\right)^2 \left(\frac{V}{h^{-3}{\rm Gpc}^3}\right)^{4/3} . \tag{12}$$

when $k_{\rm min}\ll k_{\rm max}$.

To highlight the improvement one could achieve in the future, it is useful to first calculate the detection limit for the SDSS (Sloan Digital Sky Survey) LRG sample centred at $z\sim 0.3$ and covering a volume $v\approx 2\ h^{-3}{\rm Gpc}^3$. Assuming a linear bias $b=2$ and a skewness parameter $S_3^{(1)}\sim 2\times 10^{-4}$ appropriate for halos of mass $M\sim 10^{12}-10^{13}\ {\rm M}_\odot/h$, the minimum $g_{\rm NL}$ detectable at the 1-σ level is $\simeq 10^6$ for a correction factor $\varepsilon_\kappa = 0.3$ which we read off from Fig. 5. For a survey configuration analogous to SDSS-III/BOSS [1], with central redshift $z=0.5$ and a comoving volume $V=6\ h^{-3}{\rm Gpc}^3$, the minimum $g_{\rm NL}$ would be $\sim 4\times 10^5$ for galaxies tracing halos of similar mass and bias. Finally, for a configuration like EUCLID [2], a survey of $V=100\ h^{-3}{\rm Gpc}^3$ centred at $z=1.4$, the detection limit would be $\sim 2.1\times 10^4$. Although these limits are only indicative, they show that future galaxy surveys should furnish interesting constraints on the size of the cubic coupling $g_{\rm NL}\phi^3$.

Predictions for CMB temperature anisotropies

The CMB trispectrum provides an alternative probe of local, non-quadratic correction to the Gaussian curvature perturbations, so it is interesting to assess the sensitivity of this statistics to the nonlinear parameter $g_{\rm NL}$.

Once the temperature anisotropy field is decomposed into spherical harmonics, $\Delta T(\hat{\mathbf{n}})/T = \sum_{lm} a_l^m Y_l^m(\hat{\mathbf{n}})$, an estimator for the CMB trispectrum $T_{l_3 l_4}^{l_1 l_2}(L)$ can be formed from the 4-point correlation of the spherical harmonic coefficients a_l^m. For this estimator, the signal-to-noise summed up to a certain $l_{\rm max}$ is [23, 24]

$$\left(\frac{S}{N}\right)^2 (<l_{\rm max}) \approx f_{\rm sky} \sum_{l_1>l_2>l_3>l_4}^{l_{\rm max}} \sum_L \frac{|T_{l_3 l_4}^{l_1 l_2}(L)|^2}{(2L+1)C_{l_1}C_{l_2}C_{l_3}C_{l_4}} \tag{13}$$

when cosmic variance dominates the errors. Otherwise, one shall include a contribution from the power spectrum of the detector noise to the C_l. Galactic foreground subtraction further reduces $(S/N)^2$ by a factor of $f_{\rm sky}$. Neglecting the ISW (Integrated Sachs-Wolfe) effect, the Sachs-Wolfe provides a useful order-of-magnitude estimate of the signal-to-noise as long as $l_{\rm max}$ does not exceed $\lesssim$100. A power-law fit to the signal-to-noise ratio squared in the Sachs-Wolfe approximation gives [21]

$$\left(\frac{S}{N}\right)^2 (<l_{\rm max}) \simeq 2.43\times 10^{-17} f_{\rm sky}\, g_{\rm NL}^2 \left(\frac{A_\phi}{10^{-9}}\right)^2 l_{\rm max}^{2.6} . \tag{14}$$

Assuming that this scaling persists well beyond the range over which the Sachs-Wolfe effect dominates, the minimum $g_{\rm NL}$ detectable at 1-σ level is $g_{\rm NL}\simeq 20$, 7.9, 3.2, 1.9 and 1.3×10^4 for $l_{\rm max}=250$, 500, 1000, 1500 and 2000. We have

[1] www.sdss3.org
[2] http://sci.esa.int/science-e/www/object/index.cfm?fobjectid=42266

also assumed $f_{\rm sky} = 1$. A more realistic calculation should include the full radiation transfer function, detector noise etc. For the WMAP CMB temperature measurement [3] ($l_{\rm max} \sim 250$), no detection of a significant trispectrum implies $|g_{\rm NL}| \leq 2 \times 10^5$ at the 1-σ level. This is of the same order as the limit we derived from the QSO sample analyzed by [4]. For a PLANCK-like experiment [4] ($l_{\rm max} \sim 1500$), no evidence for a trispectrum would imply $|g_{\rm NL}| \leq 1.3 \times 10^4$ at the 1-σ level. This is comparable to the detection limit that could be achieved with an all-sky survey such as EUCLID.

CONCLUSIONS

The scale dependence of clustering of biased tracers of the density field has emerged as a powerful method to constrain the amount of primordial non-Gaussianity of the local type.

On the observational side, Ref. [4] has already applied the method to a sample of highly biased LRGs and QSOs, with mean bias $b(M) \sim 1.8$ and 2.7, respectively. As we see from Figure 3, theoretical predictions are in very good agreement with the simulations for these values of bias and scales. Hence, we expect their limits remain unchanged.

Using the compilation of LSS data used in [4], we obtain a bound on $g_{\rm NL}$ of $-3.5 \times 10^5 < g_{\rm NL} < +8.2 \times 10^5$ (at 95% CL). These are the first limits derived on $g_{\rm NL}$. While they are too weak to provide interesting constraints on inflationary scenarios such as the curvaton model, future all-sky redshift surveys should improve them by a factor of ~ 100. Future CMB observations, including PLANCK, should also improve the limits derived here by at least an order of magnitude. Given the potential for improvement, realistic models of cubic type non-Gaussianity should be tested with real observations in the next decade.

The extent to which one can improve the limits using LSS data will strongly depend on our ability to minimize the impact of sampling variance caused by the random nature of the wavemodes, and the shot-noise caused by the discrete nature of the tracers. By comparing differently biased tracers of the same surveyed volume [7] and suitably weighting galaxies (e.g. by the mass of their host halo) [25, 26], it should be possible to circumvent these problems and further improve the detection level.

To conclude, we note that the lowest order, k-dependent corrections to the Gaussian bias induced by the quadratic and the cubic coupling are fully degenerated in the halo power spectrum. It is unclear whether higher order corrections could help breaking such a degeneracy. Clearly however, it will be very valuable to measure higher statistics of biased tracers, such as the bispectrum [27, 28], as they carry much more information about the shape of the three-point function of primordial curvature perturbations than the power spectrum.

ACKNOWLEDGMENTS

We acknowledge support from the Swiss National Foundation under contract No. 200021-116696/1.

REFERENCES

1. E. Komatsu, J. Dunkley, M. R. Nolta, C. L. Bennett, B. Gold, G. Hinshaw, N. Jarosik, D. Larson, M. Limon, L. Page, D. N. Spergel, M. Halpern, R. S. Hill, A. Kogut, S. S. Meyer, G. S. Tucker, J. L. Weiland, E. Wollack, and E. L. Wright, *ApJS* **180**, 330–376 (2009), 0803.0547.
2. N. Dalal, O. Doré, D. Huterer, and A. Shirokov, *Phys. Rev. D* **77**, 123514–+ (2008), 0710.4560.
3. S. Matarrese, and L. Verde, *Astrophys. J. Lett.* **677**, L77–L80 (2008), 0801.4826.
4. A. Slosar, C. Hirata, U. Seljak, S. Ho, and N. Padmanabhan, *Journal of Cosmology and Astro-Particle Physics* **8**, 31–+ (2008), 0805.3580.
5. C. Carbone, L. Verde, and S. Matarrese, *Astrophys. J. Lett.* **684**, L1–L4 (2008), 0806.1950.
6. P. McDonald, *Phys. Rev. D* **78**, 123519–+ (2008), 0806.1061.
7. U. Seljak, *Physical Review Letters* **102**, 021302–+ (2009), 0807.1770.
8. P. McDonald, and U. Seljak, *ArXiv e-prints* (2008), 0810.0323.
9. V. Desjacques, U. Seljak, and I. T. Iliev, *Mon. Not. R. Astron. Soc.* **396**, 85–96 (2009), 0811.2748.
10. A. Taruya, K. Koyama, and T. Matsubara, *Phys. Rev. D* **78**, 123534–+ (2008), 0808.4085.

[3] http://map.gsfc.nasa.gov/
[4] http://sci.esa.int/science-e/www/area/index.cfm?fareaid=17

11. M. Sasaki, J. Väliviita, and D. Wands, *Phys. Rev. D* **74**, 103003–+ (2006), arXiv:astro-ph/0607627.
12. K. Enqvist, and T. Takahashi, *Journal of Cosmology and Astro-Particle Physics* **9**, 12–+ (2008), 0807.3069.
13. Q.-G. Huang, and Y. Wang, *Journal of Cosmology and Astro-Particle Physics* **9**, 25–+ (2008), 0808.1168.
14. Q.-G. Huang, *Journal of Cosmology and Astro-Particle Physics* **11**, 5–+ (2008), 0808.1793.
15. P. Chingangbam, and Q.-G. Huang, *Journal of Cosmology and Astro-Particle Physics* **4**, 31–+ (2009), 0902.2619.
16. Q.-G. Huang, *Journal of Cosmology and Astro-Particle Physics* **6**, 35–+ (2009), 0904.2649.
17. C. T. Byrnes, and G. Tasinato, *Journal of Cosmology and Astro-Particle Physics* **8**, 16–+ (2009), 0906.0767.
18. W. H. Press, and P. Schechter, *Astrophys. J.* **187**, 425–438 (1974).
19. S. Matarrese, L. Verde, and R. Jimenez, *Astrophys. J.* **541**, 10–24 (2000), arXiv:astro-ph/0001366.
20. M. Lo Verde, A. Miller, S. Shandera, and L. Verde, *Journal of Cosmology and Astro-Particle Physics* **4**, 14–+ (2008), 0711.4126.
21. V. Desjacques, and U. Seljak, *ArXiv e-prints* (2009), 0907.2257.
22. T. Y. Lam, R. K. Sheth, and V. Desjacques, *ArXiv e-prints* (2009), 0905.1706.
23. W. Hu, *Phys. Rev. D* **64**, 083005–+ (2001), arXiv:astro-ph/0105117.
24. T. Okamoto, and W. Hu, *Phys. Rev. D* **66**, 063008–+ (2002), arXiv:astro-ph/0206155.
25. A. Slosar, *Journal of Cosmology and Astro-Particle Physics* **3**, 4–+ (2009), 0808.0044.
26. U. Seljak, N. Hamaus, and V. Desjacques, *ArXiv e-prints* (2009), 0904.2963.
27. D. Jeong, and E. Komatsu, *ArXiv e-prints* (2009), 0904.0497.
28. E. Sefusatti, *ArXiv e-prints* (2009), 0905.0717.